Received: 26 July 2021 | Revised: 8 November 2021 | Accepted: 31 January 2022

IET Power Electronics

DOI: 10.1049/pel2.12259

The Institution of Engineering and Technology WILEY

ORIGINAL RESEARCH

A computationally efficient hybrid optimization-based model predictive control for inductive power transfer systems

Lingling Cao[1] | **Wenying Sun**[1] | **Junping He**[1] | **Ka-Hong Loo**[2]

[1]School of Mechanical Engineering and Automation, Harbin Institute of Technology, Shenzhen, China

[2]Department of Electronic and Information Engineering, The Hong Kong Polytechnic University, Hung Hom, Hong Kong

Correspondence
Junping He, School of Mechanical Engineering and Automation, Harbin Institute of Technology, Shenzhen 518055, China.
Email: hejunping@hit.edu.cn

Funding information
GuangDong Basic and Applied Basic Research Foundation, Grant/Award Number: 2019A1515110890; Shenzhen Fundamental Research Program, Grant/Award Number: GXWD20201230155427003-20200823111955001

Abstract

Model predictive control (MPC) has been actively researched in recent years for power electronics applications due to its intuitive concept, flexibility, and superior dynamic performance. However, current research on MPC for inductive power transfer (IPT) systems is rather limited. Several emerging applications such as dynamic electric vehicle charging, vehicle-to-grid services, and ad hoc power transfer between mobile devices require IPT systems to possess fast dynamic response characteristic. Here, a new MPC method based on computationally efficient hybrid optimization scheme is proposed to meet the needs of these applications. The proposed MPC method adaptively selects the moving discretized control set-based optimization or the newly proposed group-based optimization under different system's states to minimize the number of iterations required for determining the optimum control variable, thus offering the advantage of low computational burden. The paper also proposes a new prediction error compensation scheme that effectively improves the control accuracy of the proposed MPC method. All the proposed works are experimentally verified on a laboratory prototype.

1 | INTRODUCTION

Inductive power transfer (IPT) represents a more reliable, more flexible and safer power conversion method due to the elimination of physical contacts [1–4]. The power transfer technology has been increasingly used in many emerging applications, such as electric vehicles, implantable medical equipment, consumer electronics and underwater devices. Nevertheless, as IPT systems are very sensitive to parameter variations, such as variations of coupling coefficient and load resistance and operating environment, closed-loop control is required to ensure a stable and efficient power conversion in IPT systems.

One of the most commonly used control methods in IPT systems is PI control with phase-shift modulation (PI+PSM) [5–10]. However, this method fails to achieve satisfactory performance for applications requiring fast dynamic response, resulting in large overshoot/undershoot and long settling time accompanied by noticeable power oscillations. Frequent power oscillations in IPT systems will give rise to electromagnetic interference problems, which can degrade the operation and performance of motors, batteries and other electrical equipment connected to it. In addition, poor dynamic performance will also degrade system efficiency, shorten the service lifetime of the connected electrical equipment and even damage them [11]. Therefore, it is of great importance to improve the dynamic performance of IPT systems.

In order to optimize the dynamic performance of IPT systems, researchers had proposed various control strategies. In [12], a buck converter is inserted between the PFC rectifier and a conventional IPT stage, and a control strategy combining one cycle control and proportional derivative control (OCC-PD) is applied to regulate the output voltage of the buck converter for achieving a reduced settling time and output voltage overshoot. However, the existence of an additional buck converter increases the system's volume and size. An optimized PID control design method is proposed in [13]. With this method, the controller's PID gains are optimized by using multi-objective genetic algorithm. Although the system's overall dynamic performance is improved, the designed controller's performance is still limited by the inherent characteristics of PID controller. Compared with PID controller, sliding model control (SMC) is able to achieve more superior dynamic performances in

response to step parameter changes [14]. However, the modeling process is complex which greatly complicates the controller design. A switching control strategy is proposed in [15], which is effective in improving the dynamic response of IPT systems against large disturbances and suppressing primary-side current overshoot. However, the modeling process is very complex, and the switching frequency is required to be higher than the resonant frequency.

MPC is a promising control strategy for various power converters and drive applications, such as DC–AC inverters [16], AC–DC rectifiers [17], and induction motor drives [18]. It uses a mathematical model to predict a system's future behavior and selects the optimum control sequence that minimizes a specified cost function over a certain prediction horizon, thus ensuring a fast dynamic response of the system against external disturbances [19]. MPC is generally divided into two categories, continuous control set MPC (CCS-MPC) and finite control set MPC (FCS-MPC). As for IPT systems, CCS-MPC has been applied to bidirectional IPT (BIPT) systems for predicting the optimum pulse width modulation parameters for the primary and secondary bridges [20, 21]. In [22], an MPC algorithm incorporating multi-step compensation is applied to the receiver-side dc–dc converter of a dynamic IPT system for achieving fast dynamic-tracking performance. Optimum control variables are calculated analytically to meet the control objectives, namely, power control and maximum efficiency point tracking, which essentially give rise to a linear controller. As a result, system constraints and nonlinearities cannot be incorporated in the said control. FCS-MPC uses a discretized system's model to predict the future trajectory of the system's output variable(s) under the action of a finite number of control variables. It offers several advantages, such as flexibility to incorporate multiple control variables and control objectives, and suitability for application in nonlinear and constrained systems. By solving the rolling optimization problem, FCS-MPC is used in [11] and [23] for achieving fast dynamic response in BIPT systems. A large number of calculations are needed in each control interval, which incurs large computational burden.

The moving discretized control set (DCS) model predictive control (MDCS-MPC) represents the state-of-the-art of model predictive control in power converters [24], which is aimed to reduce the number of calculations needed in each switching period, leading to a lower computational burden. The method has been applied to dual-active-bridge converter [25] and can be easily adapted and applied to IPT systems. Under MDCS-MPC, the controller must gradually search for the optimum control variable by evaluating a small subset of the DCS during each control interval; hence, it is more suitable for fine-level control when the system's output is close to the steady-state value. Under large disturbances, however, MDCS-MPC may suffer from slow dynamic response, especially when the resolution of the DCS is high. This paper attempts to mitigate this problem by proposing a new MPC method for IPT systems based on hybrid optimization. The proposed MPC method retains the merits of MDCS for fine-level control near the steady-state value while introducing a new group-based optimization that greatly improves the system's dynamic performance when its output deviates significantly from the steady-state value. With group-based optimization, the full range of the control variable is discretized and divided into multiple groups and sub-groups, and a fast-search algorithm is proposed to determine a close approximation to the global optimum control variable in a time-efficient manner.

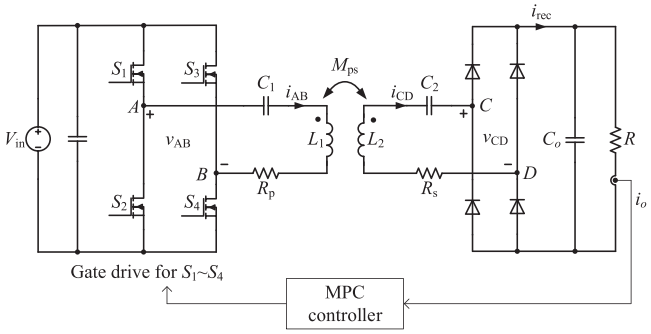

FIGURE 1 Schematic diagram of an SS-compensated IPT system

This paper is organized as follows. In Section 2, the proposed MPC method based on hybrid optimization is introduced and discussed in detail. Section 3 presents the closed-loop design of an example IPT system for realizing a stable and fast dynamic response with the proposed MPC method. By using a laboratory hardware prototype, the proposed MPC method is experimentally verified in Section 4 where its performance is thoroughly evaluated under various dynamic conditions. Finally, concluding remarks are given in Section 5.

2 | PROPOSED MODEL PREDICTIVE CONTROL BASED ON HYBRID OPTIMIZATION

Depending on the position of compensation capacitors, IPT systems are classified into four main categories, namely series–series (SS), series–parallel (SP), parallel–parallel (PP), and parallel–series (PS) topologies. Specifically, when self-inductances are SS-compensated, the values of the compensation capacitors are independent of the coupling conditions and the tank's input impedance is resistive so that circulating current and conduction loss are minimized [26].

The schematic diagram of a SS-compensated IPT system is shown in Figure 1, where V_{in} is the dc input voltage source; L_1 and L_2 are the self-inductance of the primary and secondary winding, respectively; R_p and R_s are the equivalent series resistance of the primary and the secondary winding, respectively; M_{ps} is the mutual inductance of the primary and secondary windings; C_1 and C_2 are the compensation capacitor for L_1 and L_2, respectively, which also provide dc blocking function. Finally, C_o is the output filter capacitance, and R is the load resistance.

Figure 2 depicts the primary-side inverter's gate drive signals (v_{G1}–v_{G4}) and output voltage (v_{AB}) and current (i_{AB}) waveforms. As shown in Figure 2, the gate drive signals v_{G1} and v_{G2} of switches S_1 and S_2 are complementary. Likewise, the gate

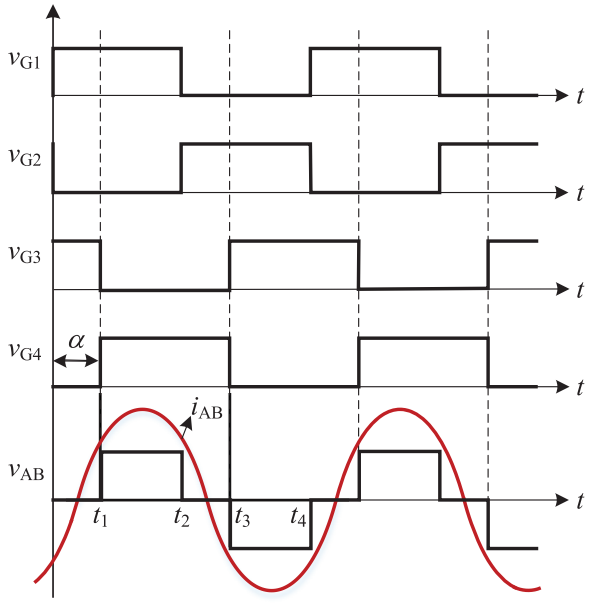

FIGURE 2 Inverter's gate drive signals (v_{G1}-v_{G4}), output voltage (v_{AB}) and output current (i_{AB})

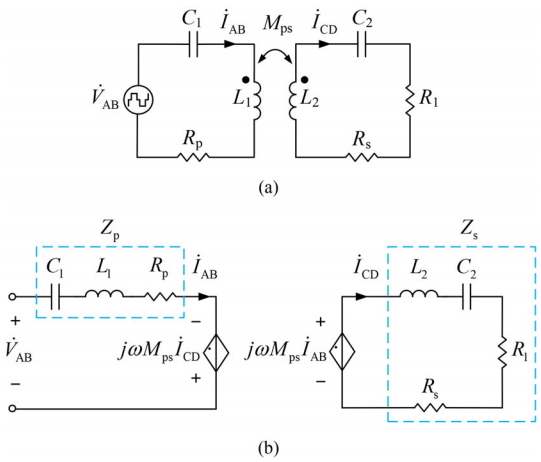

FIGURE 3 (a) Equivalent circuit model of an SS-compensated IPT system. (b) Replacement of transformer by mutual inductance model

drive signals v_{G3} and v_{G4} of switches S_3 and S_4 are also complementary, and $\alpha = DT_s$ is the phase-shift angle between v_{G1} and v_{G4}, where T_s is the switching period. The phase-shift angle α defines the duty cycle of the inverter's output voltage, which is used to control the power delivered to the rectifier and load resistance.

For simplified circuit analysis, an SS-compensated IPT system can be represented by the equivalent circuit model shown in Figure 3, where the inverter is replaced by an ideal ac voltage source v_{AB} and the rectifier and load resistance are collectively represented by an equivalent ac resistance R_1. The modeling objective is to derive a dynamic circuit model that will predict the trajectory of the converter's output current i_o as a function of the control variable during transient process.

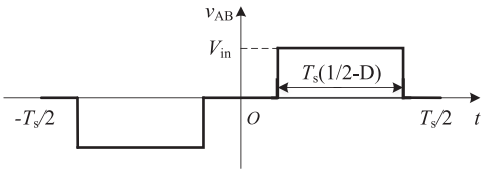

FIGURE 4 One switching cycle of inverter's output voltage (v_{AB}) waveform

According to Figure 3, Z_p and Z_s represent the input impedance of the primary and secondary circuit, respectively, with which the SS-compensated IPT system can be mathematically expressed in the following matrix form:

$$\begin{bmatrix} \dot{V}_{AB} \\ 0 \end{bmatrix} = \begin{bmatrix} Z_p & -j\omega M_{ps} \\ -j\omega M_{ps} & Z_s \end{bmatrix} \begin{bmatrix} \dot{I}_{AB} \\ \dot{I}_{CD} \end{bmatrix} \tag{1}$$

From (1), the relationship between $\dot{V}_{AB}$ and $\dot{I}_{CD}$can be obtained as given by (2):

$$\dot{I}_{CD} = j\frac{\omega M_{ps}}{Z_p Z_s + \omega^2 M_{ps}^2}\dot{V}_{AB} \tag{2}$$

To simplify the model, the equivalent series resistance of the primary winding Z_p is assumed to be zero. This condition is satisfied when$2\pi f_S = 1/\sqrt{L_1 C_1} = 1/\sqrt{L_2 C_2}$, where f_s is the switching frequency. Hence, (2) can be simplified as:

$$\dot{I}_{CD} = j\frac{1}{\omega M_{ps}}\dot{V}_{AB} \tag{3}$$

which shows that the IPT system has a constant output current characteristic with its magnitude being proportional to the primary-side inverter's output voltage.

Figure 4 shows the inverter's output voltage (v_{AB}) waveform in one switching period. By applying Fourier series analysis, the fundamental component of v_{AB} is given by (4):

$$v_{AB}(t) = \frac{4V_{in}\cos(\pi D)}{\pi}\sin(\omega t) \tag{4}$$

By combining (3) and (4), i_{CD}, that is, current on the secondary winding can be obtained as given by (5), which is rectified by the four-diode rectifier to produce the rectified current i_{rec}. To obtain the low-frequency behavior of i_{rec}, the full-wave rectified i_{rec} is averaged over one switching period to produce the average rectifier's output current $< i_{rec} >_{T_S}$ as given by (6):

$$i_{CD}(t) = \frac{4V_{in}\cos(\pi D)}{\pi\omega M_{ps}}\sin\left(\omega t + \frac{\pi}{2}\right) \tag{5}$$

$$\langle i_{rec}(t)\rangle_{T_s} = \frac{1}{T_s}\int_0^{T_s}\left|i_{CD}(t)\right| dt = \frac{4V_{in}}{\pi^3 M_{ps} f_s}\cos(\pi D) \tag{6}$$

A first-order dynamic model describing the dynamic behavior of the output *RC* filter can now be established as given by (7). Note that all quantities are switching-cycle-averaged quantities for capturing the low-frequency ($<< f_s$) behavior of the converter:

$$C_o \frac{d}{dt}\left(\langle i_o(t)\rangle_{T_s} R\right) = \langle i_{rec}(t)\rangle_{T_s} - \langle i_o(t)\rangle_{T_s} \tag{7}$$

By discretizing (7) using forward difference approximation, the discretized form of (7) can be obtained as given by (8), where k is the time step equal to a switching period:

$$I_o[k+1] = \frac{I_{rec}[k] - I_o[k]}{C_o R f_s} + I_o[k] \tag{8}$$

Finally, by substituting (6) into (8), the converter's output current at the next (i.e. k+1) time step can be expressed in terms of the duty cycle $D[k]$ and output current $i_o[k]$ values at the current time step. The equation will be used as the predictive model for implementing the proposed MPC method:

$$I_o[k+1] = \frac{4V_{in}}{f_s^2 \pi^3 M_{ps} C_o R}\cos(\pi D[k]) + \left(1 - \frac{1}{C_o R f_s}\right) I_o[k] \tag{9}$$

2.1 | Moving discretized control set model predictive control

This section briefly reviews the MDCS-MPC method proposed in [24] in the context of an SS-compensated IPT system. MDCS-MPC controls the output current i_o of the IPT system based on the discretized dynamic model of i_o given by (9). For illustration, a simple cost function is defined as given by (10) for regulating the output current i_o to track the reference current value I_{ref}. More complex cost function can be defined for multi-objective control of the IPT system:

$$ct = \left|I_{ref} - I_o[k+1]\right| \tag{10}$$

According to (9) and (10), the duty cycle D[k] is used as the control variable for output current regulation.

As MPC is generally implemented on digital controller platform, the duty cycle must be discretized into a finite set of values. Assuming that $\Delta d = f_s/f_c$ is the finest duty cycle step size that can be realized by the selected digital controller platform, where f_c is the peripheral clock frequency of the digital controller platform. The discretized D will take one of the μ_m ($= 0.5/\Delta d + 1$) values from the following set:

$$D \in \{0, \Delta d, 2\Delta d, \ldots, 0.5\} \tag{11}$$

By using (9), the controller evaluates the duty cycle in set (11) and identifies the one that minimizes the cost function (10). Here, the controller has a choice of evaluating all or some of the duty cycle values in set (11). However, considering the computational burden involved, in practice only a subset of (11) is evaluated by MDCS-MPC in each time step, and the duty cycle that gives rise to the smallest cost function is applied to the IPT system in the next time step. Assuming that $\mu = 3$ ($\mu \le \mu_m$) points are evaluated centering at the working point D of the previous time step, the resulting DCS thus consists of {$D-\Delta d$, D, $D+\Delta d$}.

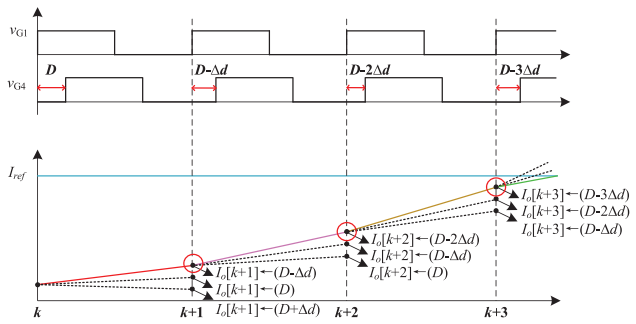

FIGURE 5 Operating principle of MDCS-MPC for IPT system ($\mu = 3$)

As shown in Figure 5, during the control interval k to k+1, controller evaluates the cost function (10) using the predicted output current obtained from (9) for the time instance k+1. Assuming that $D-\Delta d$ gives rise to the smallest cost function, the duty cycle $D-\Delta d$ is applied to the IPT system at the time instance k+1. During the next control interval k+1 to k+2, the same process repeats and the controller evaluates another three points centering at $D-\Delta d$, that is, {$D-2\Delta d$, $D-\Delta d$, D}. Assuming that $D-2\Delta d$ gives rise to the smallest cost function, the duty cycle $D-2\Delta d$ is applied to the IPT system at the time instance k+2. The same process will continue indefinitely.

It should be noted that, in order to prevent the output current to oscillate about the reference output current I_{ref}, Δd should be kept sufficiently small, and thus it tends to decrease the dynamic response of the converter if only a small number of points are evaluated during each control interval. On the contrary, evaluation of a large number of points during each control interval tend to increase the computational burden of the controller, which will also decrease the dynamic response of the converter by requiring it to operate at a lower switching frequency. Although the abovementioned problem can be partially mitigated by introducing an adaptive duty cycle Δd_{adapt} [24], which increases linearly with the difference between the sampled and reference output current (ΔI), that is, $\Delta d_{adapt} = \Delta d(1 + \lambda \Delta I)$, the linear multiplier λ needs to be determined empirically by iterative tuning, which makes it inconvenient to use in practice.

2.2 | Group-based optimization model predictive control

Here, a computationally efficient group-based optimization method is proposed to find a close approximation to the global

optimum duty cycle that minimizes the cost function during each control interval by evaluating a reduced number of points. Under MDCS-MPC, the controller must gradually search for the optimum duty cycle by evaluating a small subset of (11) during each control interval, which is time consuming, as it may take many control intervals before the optimum duty cycle is reached, especially in the case where the discretization step Δd is small. As a result, the time taken to reach the new steady state during transient process is a function of the difference between the initial and final duty cycles. It thus follows that MDCS-MPC typically does not perform well under large step disturbances. On the contrary, the proposed group-based optimization model predictive control (GBO-MPC) obtains a close approximation to the global optimum duty cycle by evaluating a reduced and fixed number of points in set (11) regardless of the initial and final states of the system. The following example illustrates the operating principle of the proposed GBO-MPC.

Assume the duty cycle range [0, 0.5] is discretized into a set of 27 values with $\Delta d = 0.5/26$. As shown in Figure 6, the 27 values are divided into three groups each consisting of nine values, which are further divided into three groups each consisting of three values. During each control interval, all 27 points are evaluated in three levels. In Level 1, the mid-points of the three groups, that is, the 5th, 14th, and 23rd points, are evaluated. The point that results in the smallest cost is selected and its group is further assessed in Level 2. Assume that the 14th point satisfies this criterion. In Level 2, the mid-points of the three subgroups belonging to this group, that is, the 11th, 14th, and 17th points, are evaluated. Similar to Level 1, the point that results in the smallest cost is selected and the group to which this point belongs is further assessed in Level 3. Assume that the 17th point satisfies this criterion. In Level 3, each subgroup consists of three points only, that is, the 16th, 17th, and 18th points, which are evaluated to determine the point that results in the smaller cost. By now, the evaluation has been completed and the optimum point (the 18th point) is obtained. The duty cycle corresponding to the optimum point is applied to the IPT system at the next time instance which drives the system's output current closest to the reference current.

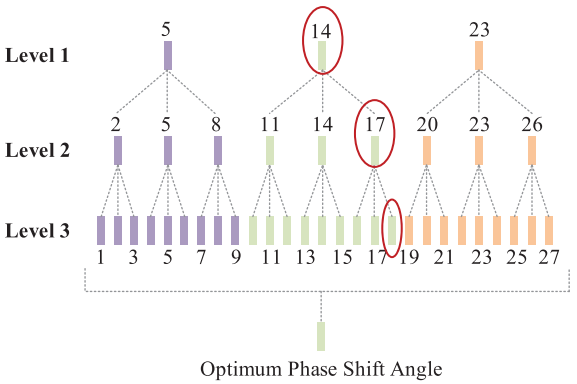

FIGURE 6 Implementation example of group-based optimization MPC

One of the greatest advantages of group-based optimization is that the number of points to be evaluated is dependent on the grouping arrangement only. Therefore, for a fixed grouping arrangement, the number of points to be evaluated is also fixed during each control interval and independent of the system's state, which greatly reduces the computational burden of the controller and enables the realization of very fast dynamic response, as will be verified in Section 4. It also simplifies the system's hardware requirement and leads to saving in system cost while maintaining a high control performance.

It can be shown that the cost function (10) is a quasi-convex function having a global minimum point equal to zero. For a function existing in this form, the global optimum duty cycle that drives the cost function to zero can be precisely found by standard search algorithms such as hill-climbing algorithm; however, it will typically take many steps to find this global optimum duty cycle, especially when the initial duty cycle is far from the global optimum value.

With the proposed GBO-MPC, the search time can be reduced significantly, although for the quasi-convex function (10) the search could only return a quasi-global optimum value that exists in the neighborhood of the actual global optimum value. Thus, the quasi-global optimum value can be considered as a close approximation to the actual global optimum value. Consequently, it is expected that the control performance of an IPT system will be degraded if it is implemented with GBO-MPC alone due to the error introduced. This problem is mitigated by unifying the merits of GBO-MPC and MDCS-MPC here. Since GBO-MPC is computationally efficient, it is suitable for coarse-level control that helps to drive the output current rapidly to the neighborhood of the reference current. MDCS-MPC, which is essentially a hill-climbing algorithm, is capable of fine-level control and is therefore subsequently invoked to further drive the output current into equality with the reference current. By means of a more precise search, MDCS-MPC also helps to eliminate any error that is introduced earlier by GBO-MPC during the coarse-level control stage.

It should be noted that the search tree depicted in Figure 6 can be expanded into more branches. If the range is discretized into 3^n values, the 3^n values are divided into three groups each consisting of 3^{n-1} values, which are evaluated in n levels. In order to obtain the quasi-global optimum duty cycle, $2n+1$ points will need to be evaluated, whereas at most $(3^{n-1} - 1)/2$ additional points will need to be evaluated for finding the global optimum duty cycle, making the total number of calculations equal to $2n+1+(3^{n-1}-1)/2$. Hence, the maximum error between the quasi-global optimum and the global optimum is $\Delta e = \Delta d(3^{n-1} - 1)/2$, where $\Delta d = 0.5/(3^n - 1)$. Although a higher control resolution can be achieved with a larger n, that is, a larger number of groups, more points will need to be evaluated in each control interval, thus consuming more computational time, and the maximum error will increase slightly with n. These factors should be weighed carefully when determining the group size for GBO-MPC.

From another perspective, today's microcontrollers or digital signal processors are capable of realizing high control resolution characterized by very small discretization step Δd, which inevitably leads to a large number of points to be evaluated if MDCS-MPC is implemented alone, especially when the error signal is large, that is, the controlled variable deviates significantly from the reference value. On the other hand, the number of points to be evaluated by GBO-MPC is fixed and independent of the error signal; thus, it is not computationally efficient to do so when the error signal is small, as it will typically take MDCS-MPC fewer steps to achieve precise output regulation close to the reference value. Therefore, an adaptive MPC should be formulated to take advantage of the shorter evaluation time and larger control variable's step size of GBO-MPC when the error signal is large, and of the shorter evaluation time of MDCS-MPC when the error signal is small, which is the objective of this paper.

Here, a hybrid *MDCS+GBO-MPC* method is proposed to meet the stated objective. With the proposed method, a threshold error value *error_m* is predefined above and below which GBO-MPC and MDCS-MPC are activated, respectively, to constantly minimize the number of points to be evaluated under all conditions. Since the maximum error between the approximate and the actual global optimum duty cycle is Δe, *error_m* should be set larger than the maximum deviation of the output current resulting from Δe, that is, $error\_m > \max\left|I_o[k+1]\right|_{D+\Delta e} - I_o[k+1]\left|_D\right|$. The advantage of the proposed method is that the barrier for the system to operate at higher switching frequency is removed and a fast dynamic response can be achieved.

2.3 | Compensation loop for prediction error correction

It should be that the output current predicted by the idealized Equation (9) tends to deviate from the sampled output current due to the presence of unmodeled parameters or parameter mismatches. If the prediction error is not compensated, it will accumulate over time and have negative impact on the performance of MPC controller [27].

A feedback loop can be implemented to compensate for the prediction error and minimize the difference between the predicted and sampled output current. When formulating the feedback loop, a compensation term Δ_c is defined by (12) as the difference between the non-compensated predicted output current calculated using (9) (denoted as I_{o_p}) and the compensated predicted output current (denoted as I_{o_c}). The term Δ_c is used to account for any unmodeled parameters or parameter mismatches present in the system. Another term Δ_s is defined by (13) as the difference between the sampled output current (denoted as I_{o_s}) and the compensated predicted output current (denoted as I_{o_c}). The control objective of the feedback loop is to reduce Δ_s to zero:

$$\Delta_c[k] = I_{o\_c}[k] - I_{o\_p}[k] \tag{12}$$

$$\Delta_s[k] = I_{o\_s}[k] - I_{o\_c}[k] \tag{13}$$

$$I_{o\_c}[k+1] = I_{o\_p}[k+1] + \left(K_p + K_i T\right)\Delta_s[k] + K_i\Delta_c[k-1] \tag{14}$$

With the above definitions, a feedback loop can be constructed as shown in Figure 7, where K_p and K_i are the proportional and integral gain, respectively. At time instance k, the error signal $\Delta_s[k]$ is obtained by subtracting the compensated predicted output current $I_{o\_c}[k]$ from the sampled output current $I_{o\_s}[k]$. The error signal is inputted to the PI compensator which produces the compensation signal $\Delta_c[k]$. Finally, the compensation signal, which accounts for the system's non-idealities, is added to the non-compensated predicted output current calculated from (9) to produce the compensated predicted output current $I_{o\_c}[k+1]$ for the next time instance $k+1$. At time instance $k+1$, $I_{o\_c}[k+1]$ is subtracted from the newly sampled output current $I_{o\_s}[k+1]$, and the same process will repeat for the subsequent time instances. Equation (14) summarizes the control action of the feedback loop.

Figure 8 shows the flowchart of the proposed hybrid MDCS+GO MPC method, where *error* is the deviation of the output current from the reference value and *error_m* denotes the threshold error value that triggers the switching between MDCS-MPC and GBO-MPC.

3 | CLOSED-LOOP OUTPUT CURRENT REGULATION

The purpose of this section is to design a conventional PI controller for achieving closed-loop output current regulation and use it as a benchmark for assessing the performances of the MDCS-MPC and the proposed hybrid MDCS-GBO-MPC methods.

To design a suitable PI compensator, a small-signal model of the IPT system should be derived. By substituting (6) into (7), the large-signal model of the IPT system is obtained as given by (15):

$$RC_o\frac{d}{dt}\left(\langle i_o(t)\rangle_{T_s}\right) = \frac{4\langle V_{in}(t)\rangle_{T_s}}{\pi^3 M_{ps} f_s}\cos\left[\pi d(t)\right] - \langle i_o(t)\rangle_{T_s} \tag{15}$$

The small-signal disturbances given by (16) are introduced into (15), where V_{in}, D, and I_o are the steady-state input voltage, duty cycle, and output current, respectively, and the

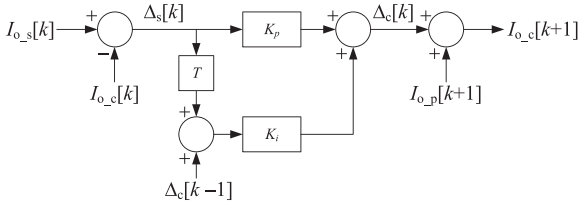

FIGURE 7 Compensation loop for prediction error correction

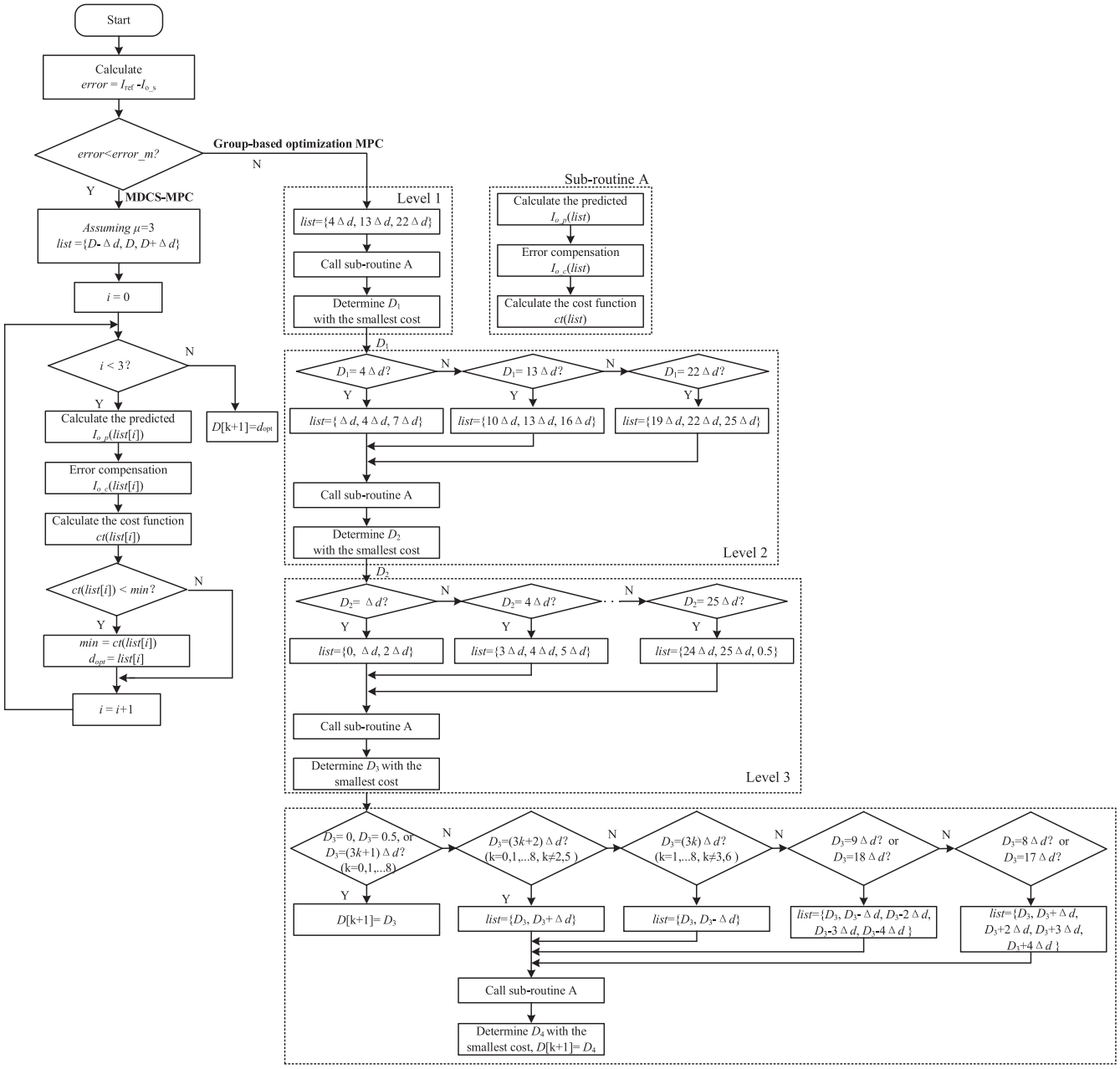

FIGURE 8 Flowchart of the proposed hybrid MDCS+GO MPC method

resulting equation is linearized by ignoring higher-order terms. The linearized equation is given by (17):

$$\begin{aligned} \langle V_{\text{in}}(t)\rangle_{T_s} &= V_{\text{in}} + \Delta v_{\text{in}}(t) \\ d(t) &= D + \Delta d(t) \\ \langle i_{\text{o}}(t)\rangle_{T_s} &= I_{\text{o}} + \Delta i_{\text{o}}(t) \end{aligned} \tag{16}$$

$$\begin{aligned} RC_{\text{o}}\frac{d\Delta i_{\text{o}}(t)}{dt} &= \frac{4V_{\text{in}}\sin(\pi D)}{\pi^2 M_{\text{ps}} f_s}\Delta d(t) \\ &+ \frac{4\cos(\pi D)}{\pi^3 M_{\text{ps}} f_s}\Delta v_{\text{in}}(t) - \Delta i_{\text{o}}(t) \end{aligned} \tag{17}$$

By taking the Laplace transform of (17), the IPT system's small-signal transfer function from duty cycle to output current is obtained as given by (18):

$$G(s) = \left.\frac{\Delta i_{\text{o}}(s)}{\Delta d(s)}\right|_{\Delta v_{\text{in}}(s)=0} = \frac{4V_{\text{in}}\sin(\pi D)}{\pi^2 M_{\text{ps}} f_s RC_{\text{o}}}\left(\frac{RC_{\text{o}}}{1+sRC_{\text{o}}}\right) \tag{18}$$

Figure 9 shows the Bode diagram of $G(s)$. As can be seen from Figure 9, the 0-dB frequency of the uncompensated system is about 200 Hz with a phase margin of about 130°. Due to the small bandwidth and over-damped characteristic of the uncompensated system, the dynamic response of the

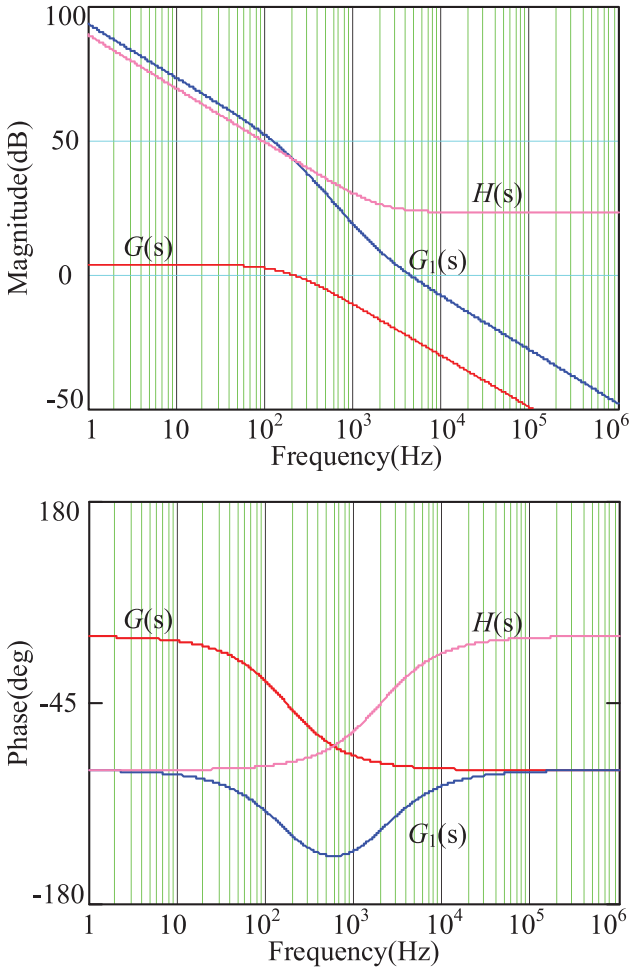

FIGURE 9 Uncompensated and compensated loop gain of the IPT system

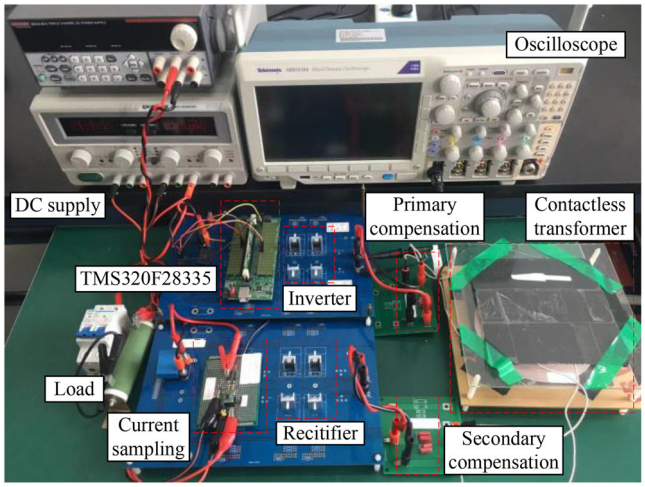

FIGURE 10 Experimental prototype

TABLE 1 Specifications of hardware prototype

Parameter	Value
Dc input voltage V_{in}	24 V
Switching frequency f_s	40 kHz
Self-inductance of the primary/secondary winding L_1/L_2	162 μH
Compensation capacitor in the primary/secondary C_1/C_2	102 nF
Output capacitor C_o	22 μF
Load resistor R	20 Ω

uncompensated system is expected to be poor. Furthermore, the uncompensated system has a small static gain, which tends to introduce a large static error to the output current, and this problem must be mitigated by increasing the system's static gain. Therefore, a PI compensator with a transfer function of $H(s) = K_p + K_i/s$ is designed to achieve a fast dynamic response as well as to eliminate the static error in the system's output current. By selecting $K_p = 8.6$ and $K_i = 108{,}100$, a new 0-dB frequency of 4 kHz (one tenth of the switching frequency) and a new phase margin of 65° is achieved for the compensated system. The Bode diagram of the compensated system $G_1(s)$ is plotted in Figure 9, from which it can be seen that a large static gain and a significantly increased system bandwidth (200 Hz → 4 kHz) have been realized by the designed PI compensator.

4 | EXPERIMENTAL VERIFICATION

To verify the effectiveness of the hybrid MDCS+GBO-MPC method proposed in this paper, a hardware prototype of 30W IPT system for battery charging has been constructed as shown in Figure 10 with the hardware specifications listed in Table 1. DC power supply 2231A-30-3 from Keithley is used as the input source. Polypropylene capacitors from Wima are used as the compensation capacitors in both primary and secondary sides. The coupling coefficient of the IPT transformer is 0.33 ($M_{ps} = 52\mu$H) with an air gap of 50 mm between the primary and secondary coils. The proposed hybrid control strategy is implemented using TMS320F28335 microcontroller. Four cases will be experimentally studied and discussed; namely, variation of dc input voltage, variation of reference output current, variation of coupling coefficient, and variation of load resistance, and detailed comparisons are made with the conventional PI control and the state-of-the-art MDCS-MPC proposed in [24]. For MDCS-MPC, $\mu = 3$ is selected; thus, three duty cycles will be evaluated during each control interval, whereas for the proposed hybrid MDCS+GBO-MPC, the duty cycle range [0, 0.5] is discretized into 27 values, among which 7 are evaluated during each control interval.

4.1 | Variation of DC input voltage

Figure 11 shows the dynamic responses of the IPT system under PI control, MDCS-MPC, and the proposed hybrid

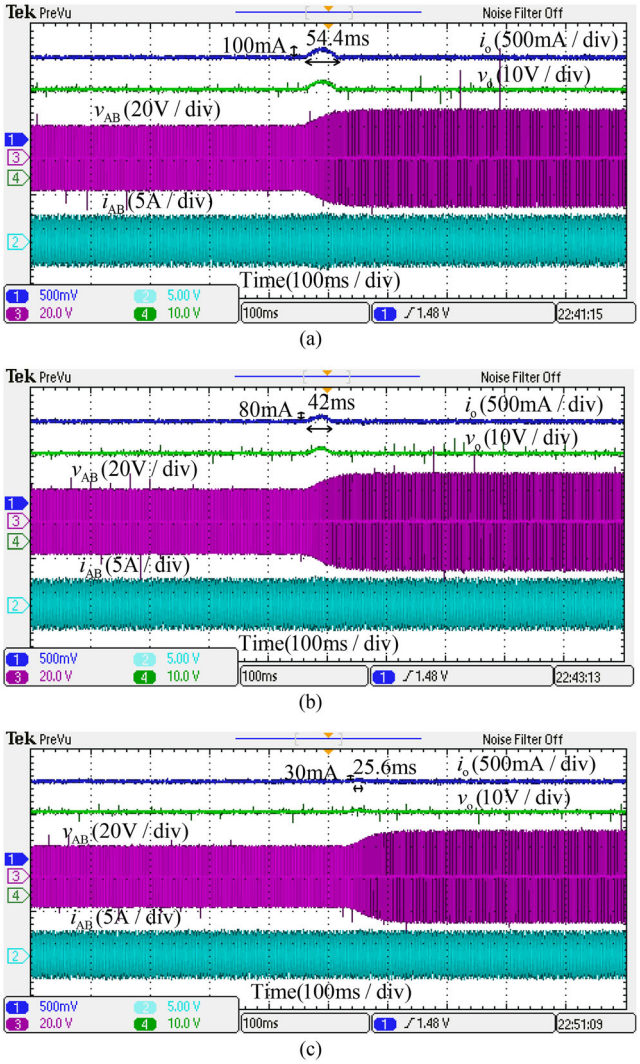

FIGURE 11 Comparison of system's dynamic responses under three closed-loop control strategies when input voltage changes from 20 to 30 V: (a) conventional PI control, (b) MDCS-MPC, and (c) proposed hybrid MDCS+GBO-MPC

MDCS+GBO-MPC when the dc input voltage changes from 20 to 30 V. In all three cases, a rapid change in the dc input voltage has caused the peak value of v_{AB} to increase proportionally. To maintain a constant output current, and hence a constant output power, delivered to the load, all three controllers act to decrease the duty cycle of v_{AB} to the same value at steady state. The difference between the three controllers lies in their dynamic performances during transient state. The output current overshoot and setting time resulting from the three controllers are summarized in Table 2. It shows that, compared to conventional PI control, the proposed hybrid MDCS+GBO-MPC has resulted in 70% and 52.9% decreases in output current overshoot and settling time, respectively, during the rapid increase in dc input voltage. Compared to the state-of-the-art MDCS-MPC, significant 62.5% and 39% decreases in output current overshoot and settling time, respectively, are also achieved by the proposed hybrid MDCS+GBO-MPC.

TABLE 2 Performance comparison between different control schemes under variation of DC input voltage

Control scheme	Overshoot (mA)	Setting time (ms)
PI	100	54.4
MDCS-MPC	80	42
MDCS+GBO-MPC	30	25.6

TABLE 3 Performance comparison between different control schemes under variation of reference output current

Control scheme	Fall time (ms)	Rise time (ms)
PI	13.2	10
MDCS-MPC	6.4	5.6
MDCS+GBO-MPC	2	1.2

The superior dynamic performance of the proposed hybrid MDCS+GBO-MPC can be explained by its efficient computation and fast identification of a close approximation to the global optimum duty cycle that minimizes the output current deviation during *every* control interval. For MDCS-MPC, as it only evaluates the few points adjacent to the previous working duty cycle (two points in this experiment in accordance with [24]) during each control interval, and the evaluated points typically do not correspond to the global optimum duty cycle unless the output current deviation is very small; it will take many more control intervals compared to the proposed hybrid MDCS+GBO-MPC to close the gap between the actual output current and the reference output current.

4.2 | Variation of reference output current

The performance of the proposed hybrid MDCS+GBO-MPC is also evaluated under variation of reference output current. In the three cases depicted in Figure 12, the reference output current is stepped from 1.2 to 0.6 A and back to 1.2 A, and Figure 12a–c shows the experimentally measured system's step responses under conventional PI control, MDCS-MPC, and the proposed hybrid MDCS+GBO-MPC, respectively. The rise time and fall time resulting from the three controllers are summarized in Table 3. With conventional PI control, the system's output current takes 13.2 and 10 ms to decrease from 1.2 to 0.6 A and increase from 0.6 to 1.2 A, respectively. These transition times have been significantly reduced to 6.4 and 5.6 ms, respectively, with MDCS-MPC. With the proposed hybrid MDCS+GBO-MPC, these transition times are further reduced to merely 2 and 1.2 ms, respectively. Despite the fast transitions between the two output current levels, no significant overshoot/undershoot or oscillation is observed, a desired feature which cannot be achieved with conventional PI control. Although MDCS-MPC is able to achieve a much faster dynamic

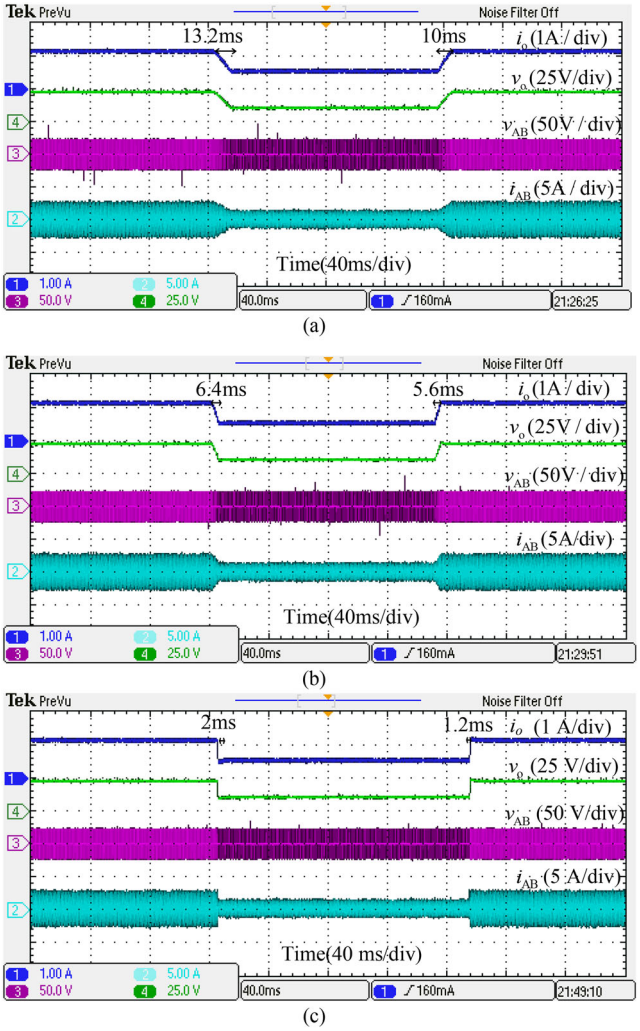

FIGURE 12 Comparison of system's dynamic responses under three closed-loop control strategies when reference output current changes from 1.2 to 0.6 A and back to 1.2 A: (a) conventional PI control, (b) MDCS-MPC, and (c) proposed hybrid MDCS+GBO-MPC

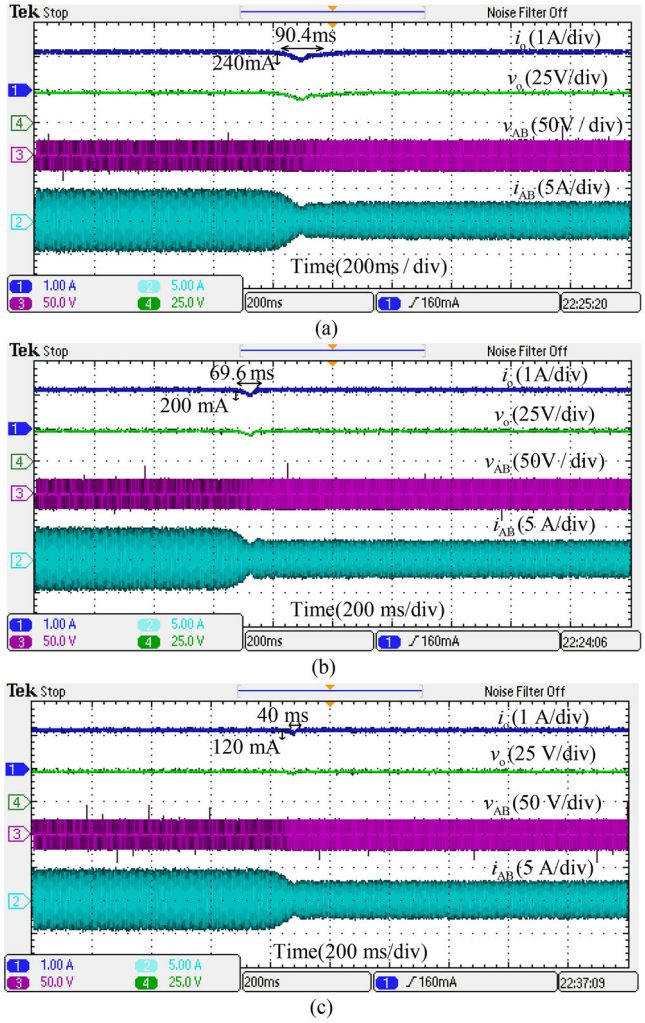

FIGURE 13 Comparison of system's dynamic responses under three closed-loop control strategies when coupling coefficient changes from 0.25 to 0.33: (a) conventional PI control, (b) MDCS-MPC, and (c) proposed hybrid MDCS+GBO-MPC

response compared to PI control, it still takes a considerable amount of time to reach the new steady state due to the relatively slow process of moving through different control sets in search of the desired duty cycle.

4.3 | Variation of coupling coefficient

A commonly encountered situation in IPT applications is the variation of coupling coefficient between the transmitter and receiver coils due to position misalignment or change in the distance between two coils, for example, in dynamic wireless charging. To emulate these situations, the coupling coefficient between the transmitter and receiver coils is changed rapidly from 0.25 to 0.33, and the experimentally measured waveforms under conventional PI control, MDCS-MPC, and the proposed hybrid MDCS+GBO-MPC are depicted in Figure 13a–c, respectively. In all three cases, the output current of the IPT system initially decreases due to the weaker coupling, and hence reduced power transfer, from the transmitter coil to the receiver coil. The decreased output current is detected by the controller which attempts to compensate for it by increasing the duty cycle of v_{AB}. With conventional PI control, the initial decrease in the output current amounts to 240 mA, that is, 20% undershoot, which only recovers after 90.4 ms. With MDCS-MPC, the initial output current undershoot has decreased to 200 mA and the settling time is shortened to 69.6 ms, that is, 23% reduction compared to PI control. In comparison to the previous two cases, the proposed hybrid MDCS+GBO-MPC has further reduced the output current undershoot and settling time to 120 mA and 40 ms, respectively. Table 4 summarizes the undershoot and settling time resulting from the three controllers. Given the much shorter settling time achieved, the proposed hybrid MDCS+GBO-MPC is suitable for applications that involve

TABLE 4 Performance comparison between different control schemes under variation of coupling coefficient

Control scheme	Undershoot (mA)	Settling time (ms)
PI	240	90.4
MDCS-MPC	200	69.6
MDCS+GBO-MPC	120	40

TABLE 5 Performance comparison between different control schemes under variation of load resistance

Control scheme	Undershoot (mA)	Settling time (ms)
PI	350	2
MDCS-MPC	350	1.5
MDCS+GBO-MPC	350	1.2

frequent changes of coupling coefficient such as dynamic wireless charging.

4.4 | Variation of load resistance

Step load change is not a typical situation encountered in wireless charging as the equivalent resistance of battery tends to change slowly over the course of charging. However, recently, multi-load/multi-output IPT systems have attracted the interest of researchers as a more flexible wireless charging solution, especially for handheld/mobile devices [28, 29]. In multi-load IPT systems, loads can be added to or removed from the charging platform in an almost ad hoc manner, causing an abrupt change in the equivalent load resistance seen by the transmitter circuit. This situation is emulated by a step load change in the experiments conducted in this section. Figure 14a–c shows the experimental waveforms of the IPT system under conventional PI control, MDCS-MPC, and the proposed hybrid MDCS+GBO-MPC when the load resistance is stepped from 20 to 40 Ω. The output current undershoot and settling time resulting from the three controllers are summarized in Table 5. As the output capacitor's voltage cannot change abruptly, the output current experiences an initial decrease of about 350 mA in all three cases. The controller then acts to restore the output current to the reference value by increasing the duty cycle of v_{AB}. Among the three control methods being compared, the proposed hybrid MDCS+GBO-MPC has resulted in the shortest settling time (1.2 ms), followed by MDCS-MPC (1.5 ms) and conventional PI control (2 ms). The experimental results verified that MPC-based controllers are generally more superior in dynamic performance compared to PI control. Finally, the proposed hybrid MDCS+GBO-MPC is proven to perform better than the state-of-the-art MDCS-MPC due to the newly inbuilt group-based optimization feature that helps to drive the system's fast convergence to steady state.

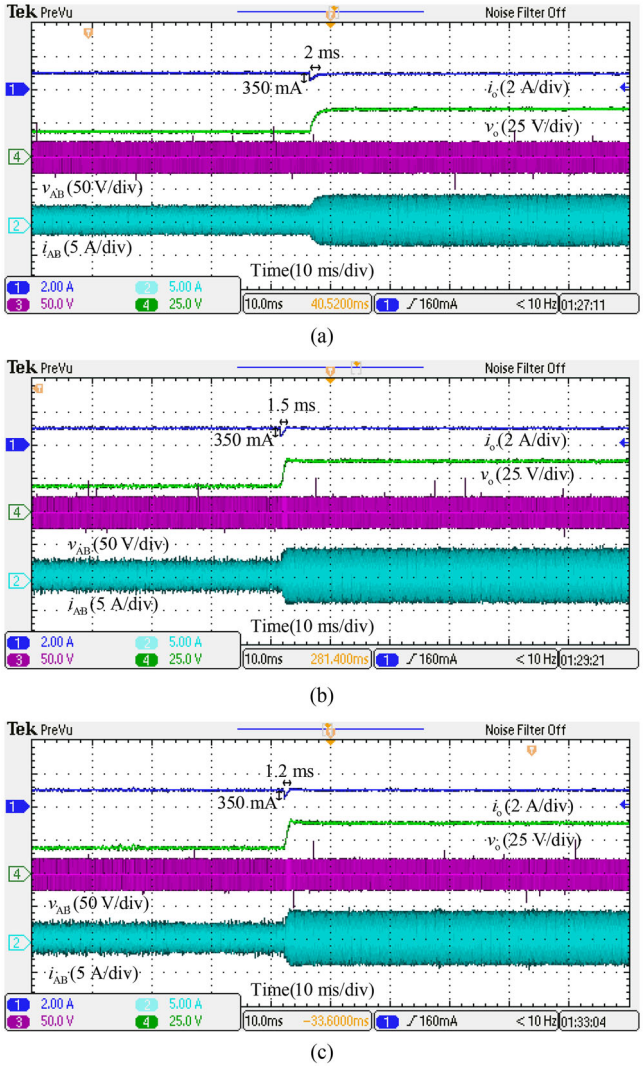

FIGURE 14 Comparison of system's dynamic responses under three closed-loop control strategies when load resistance changes from 20 to 40 Ω : (a) conventional PI control, (b) MDCS-MPC, and (c) proposed hybrid MDCS+GBO-MPC

5 | CONCLUSION

A new computationally efficient MPC method for IPT systems based on hybrid optimization is proposed here. The proposed method is formulated to switch between two optimization modes, namely, MDCS-MPC and GBO-MPC, as a function of the magnitude of output current deviation. The objective is to minimize the computational burden to search for the optimum control variable while maintaining high control accuracy and fast dynamic response under all dynamic conditions. The proposed method has been tested on a laboratory hardware prototype under variations of dc input voltage, reference output current, coupling coefficient, and load resistance, and it has been experimentally verified that the proposed MPC method has demonstrated more superior dynamic performances compared to the conventional PI control and the state-of-the-art MDCS-MPC method.

ACKNOWLEDGEMENTS

This work was supported by the GuangDong Basic and Applied Basic Research Foundation 2019A1515110890 and the Shenzhen Fundamental Research Program GXWD20201230155427003-20200823111955001.

CONFLICT OF INTEREST

No conflict of interest exits in the submission of this manuscript.

DATA AVAILABILITY STATEMENT

The data are available from the corresponding author upon reasonable request.

ORCID

Lingling Cao https://orcid.org/0000-0001-8441-7652

REFERENCES

1. Zhang, Z., Pang, H., Georgiadis, A., et al.: Wireless power transfer—an overview. IEEE Trans. Ind. Electron. 66(2), 1044–1058 (2019)
2. Cirimele, V., Diana, M., Freschi, F., et al.: Inductive power transfer for automotive applications: State-of-the-art and future trends. IEEE Trans. Ind. Appl. 54(5), 4069–4079 (2018)
3. Patil, D., McDonough, M.K., Miller, J.M., et al.: Wireless power transfer for vehicular applications: Overview and challenges. IEEE Trans. Transp. Electrif. 4(1), 3–37 (2018)
4. Mohamed, A.A.S., Lashway, C.R., Mohammed, O.: Modeling and feasibility analysis of quasi-dynamic WPT system for EV applications. IEEE Trans. Transp. Electrif. 3(2), 343–353 (2017)
5. Mai, R., Liu, Y., Li, Y., et al.: An active-rectifier-based maximum efficiency tracking method using an additional measurement coil for wireless power transfer. IEEE Trans. Power Electron. 33(1), 716–728 (2018)
6. Li, Y., Hu, J., Chen, F., et al.: Dual-phase-shift control scheme with current-stress and efficiency optimization for wireless power transfer systems. IEEE Trans. Circuits Syst. I Regul. Pap. 65(9), 3110–3121 (2018)
7. Tang, Y., Chen, Y., Madawala, U.K., et al.: A new controller for bidirectional wireless power transfer systems. IEEE Trans. Power Electron. 33(10), 9076–9087 (2018)
8. Lee, J., Han, B.: A bidirectional wireless power transfer EV charger using self-resonant PWM. IEEE Trans. Power Electron. 30(4), 1784–1787 (2015)
9. Madawala, U.K., Neath, M., Thrimawithana, D.J.: A power–frequency controller for bidirectional inductive power transfer systems. IEEE Trans. Ind. Electron. 60(1), 310–317 (2013)
10. Mohamed, A.A.S., Berzoy, A., de Almeida, F.G.N., et al.: Modeling and assessment analysis of various compensation topologies in bidirectional IWPT system for EV applications. IEEE Trans. Ind. Appl. 53(5), 4973–4984 (2017)
11. Liu, S., Mai, R., Zhou, L., et al.: Dynamic improvement of inductive power transfer systems with maximum energy efficiency tracking using model predictive control: Analysis and experimental verification. IEEE Trans. Power Electron. 35(12), 12752–12764 (2020)
12. Shi, W., Deng, J., Wang, Z., et al.: The start-up dynamic analysis and one cycle control-PD control combined strategy for primary-side controlled wireless power transfer system. IEEE Access 6, 14439–14450 (2018)
13. Neath, M.J., Swain, A.K., Madawala, U.K., et al.: An optimal PID controller for a bidirectional inductive power transfer system using multiobjective genetic algorithm. IEEE Trans. Power Electron. 29(3), 1523–1531 (2014)
14. Yang, Y., Zhong, W., Kiratipongvoot, S., et al.: Dynamic improvement of series–series compensated wireless power transfer systems using discrete sliding mode control. IEEE Trans. Power Electron. 33(7), 6351–6360 (2018)
15. Jiang, J., Song, K., Li, Z., et al.: System modeling and switching control strategy of wireless power transfer system. IEEE J. Emerg. Sel. Top. Power Electron. 6(3), 1295–1305 (2018)
16. Dragičević, T.: Model predictive control of power converters for robust and fast operation of AC microgrids. IEEE Trans. Power Electron. 33(7), 6304–6317 (2018)
17. Gao, H., Wu, B., Xu, D., et al.: Model predictive control scheme with active damping function for current source rectifiers. IET Power Electronics 10(7), 717–725 (2017)
18. Zhang, Y., Yang, H., Xia, B.: Model predictive torque control of induction motor drives with reduced torque ripple. IET Electr. Power Appl. 9(9), 595–604 (2015)
19. Kouro, S., Cortes, P., Vargas, R., et al.: Model predictive control—a simple and powerful method to control power converters. IEEE Trans. Ind. Electron. 56(6), 1826–1838 (2009)
20. Mohamed, A.A.S., Youssef, T., Mohammed, O.: Vehicle side predictive power-flow control of bidirectional WPT system for EV ancillary services. In: IEEE Applied Power Electronics Conference and Exposition (APEC), pp. 3211–3217. IEEE, Piscataway, NJ (2017)
21. Qi, C., Lang, Z., Su, L., et al.: Model predictive control for a bidirectional wireless power transfer system with maximum efficiency point tracking. In: IEEE International Symposium on Predictive Control of Electrical Drives and Power Electronics (PRECEDE), pp. 1–5. IEEE, Piscataway, NJ (June 2019)
22. Zhou, Z., Zhang, L., Liu, Z., et al.: Model predictive control for the receiving-side DC–DC converter of dynamic wireless power transfer. IEEE Trans. Power Electron. 35(9), 8985–8997 (2020)
23. Qi, C., Lang, Z., Li, T., et al.: Finite-control-set model predictive control for magnetically coupled wireless power transfer systems. Journal of Power Electronics 21, 1095–1105 (2021)
24. Chen, L., Shao, S., Xiao, Q., et al.: Model predictive control for dual-active-bridge converters supplying pulsed power loads in naval DC micro-grids. IEEE Trans. Power Electron. 35(2), 1957–1966 (2020)
25. Chen, L., Lin, L., Shao, S., et al.: Moving discretized control set model-predictive control for dual active bridge with the triple-phase shift. IEEE Trans. Power Electron. 35(8), 8624–8637 (2020)
26. Zhang, W., Wong, S.C., Tse, C.K., et al.: Design for efficiency optimization and voltage controllability of series-series compensated inductive power transfer systems. IEEE Trans. Power Electron. 29(1), 191–200 (2014)
27. Shen, K., Feng, J., Zhang, J.: Finite control set model predictive control with feedback correction for power converters. CES Trans. Electr. Mach. Syst. 2(3), 312–319 (2018)
28. Fu, M., Zhang, T., Zhu, X., et al.: Compensation of cross coupling in multiple-receiver wireless power transfer systems. IEEE Trans. Ind. Inf. 12(2), 474–482 (2016)
29. Huang, Y., Liu, C., Zhou, Y., et al.: Power allocation for dynamic dual-pickup wireless charging system of electric vehicle. IEEE Trans. Magn. 55(7), 1–6 (2019)

How to cite this article: Cao, L., Sun, W., He, J., Loo, K.-H.: A computationally efficient hybrid optimization-based model predictive control for inductive power transfer systems. IET Power Electron. 15, 689–700 (2022).
https://doi.org/10.1049/pel2.12259